SOLUTION OF ADVECTION DIFFUSION EQUATIONS IN TWO SPACE DIMENSIONS BY A RATIONAL EULERIAN LAGRANGIAN LOCALIZED ADJOINT METHOD OVER HEXAGONAL GRIDS

MOHAMED AL-LAWATIA

Abstract. We present a characteristic method for the solution of the transient advection diffusion equations in two space-dimensions. This method uses Wachspress-type rational basis functions over hexagonal grids within the framework of the Eulerian Lagrangian localized adjoint methods (ELLAM). It therefore maintains the advantages of previous ELLAM schemes and generates accurate numerical solutions even if large time steps are used in the simulation. Numerical experiments are presented to illustrate the performance of this method and to investigate its convergence numerically.

Key Words. advection-diffusion equations, characteristic methods, Eulerian-Lagrangian methods, rational basis functions

1. Introduction

Advection-diffusion equations are a class of partial differential equations that is mathematically important because they arise in many problems in Science and Engineering. These equations are also important because they present serious computational difficulties, especially when advection dominates the physical process. Standard finite difference and finite element methods, which work well for many other types of equations, generate solutions for this class of equations that exhibit non-physical spurious oscillations and/or artificial numerical diffusion that smears out sharp fronts of the solution where important chemistry and physics take place.

Many specialized methods have been developed which aim at resolving the difficulties mentioned when applied to both linear and nonlinear problems. One large class of methods, usually referred to as *characteristic methods*, makes use of the hyperbolic nature of the governing equations. These methods incorporate Eulerian grids with Lagrangian tracking along the characteristic curves to treat the advective part of the equation [9, 13]. This treatment allows for larger time steps to be used in the simulation. Moreover, it significantly reduces the time truncation errors when compared to methods which rely only on Eulerian grids. However, these methods have difficulty in conserving mass and in treating general boundary conditions.

The Eulerian Lagrangian localized adjoint method was developed by Celia, Russell, Herrera, and Ewing as an improved extension of characteristic methods which maintains their advantages and enhances their performance by conserving mass and treating general boundary conditions naturally in its formulation [6]. This first ELLAM formulation was a finite element formulation for one-dimensional constant

---

coefficient advection diffusion equations. The strong potential that this formulation has shown, led to a rapid expansion in all aspects of this class of methods, including the development of various finite element and finite volume formulations for one and higher dimensional problems [1, 3, 10, 14, 26, 27]. Other formulations were also developed including Eulerian-Lagrangian collocation methods [39, 40, 41], and Eulerian Lagrangian discontinuous Galerkin methods [34, 35, 36, 37]. Moreover, convergence properties of the different ELLAM formulations were studied and various optimal order convergence and uniform estimates were established [19, 20, 21, 22, 23, 24, 25, 30, 31, 32, 33].

ELLAM formulations developed for two-dimensional problems have mostly followed the classical polynomial-based finite element approach; which is to discretize the spatial domain into an assembly of triangular or quadrilateral elements and use linear or higher polynomial interpolants as the test functions on each element and the basis for the solution space [12]. However, due to the reliance on polynomial basis, other types of higher-order elements have not been extensively considered even though such elements with large number of sides have been successfully used in a number of applications in Engineering and other fields and have resulted in some cases in better approximations than those obtained by triangular or quadrilateral polynomial based standard finite element codes [7].

In this article we present a rational characteristic method for the solution of variable coefficient advection diffusion equations within the framework of the Eulerian-lagrangian localized adjoint methods. The algorithm is based on a discretization of the spatial domain into a partition of regular hexagonal elements and uses Wachspress-type rational test functions in the space-time domain defined by the characteristics [18]. The derived method generates regularly structured systems which can easily be solved numerically. Numerical experiments are presented to illustrate the performance of the method developed.

2. Development of the Characteristic Schemes

We consider the following two-dimensional unsteady-state advection diffusion equation

$$(1) \qquad (\phi(\mathbf{x}, t)\, u(\mathbf{x}, t))_t + \nabla \cdot \Big(\mathbf{v}(\mathbf{x}, t) u(\mathbf{x}, t) - \mathbf{D}(\mathbf{x}, t) \nabla u(\mathbf{x}, t) \Big) = f(\mathbf{x}, t)$$

where $\mathbf{x} = (x, y)$, $u_t = \partial u / \partial t$, $\nabla = \langle \partial / \partial x, \partial / \partial y \rangle$, $\phi(\mathbf{x}, t)$ is the retardation coefficient, $\mathbf{v}(\mathbf{x}, t)$ is the velocity field, $\mathbf{D}(\mathbf{x}, t)$ is the diffusion/dispersion tensor, and $f(\mathbf{x}, t)$ is a source/sink term. While the ELLAM method can be developed for any bounded spatial domain which admits a quasi-uniform partition, for simplicity of presentation we consider a spatial domain of the form $\Omega = [a, b] \times [c, d]$. To close the system, we assume that an appropriate initial condition and any proper combination of Dirichlet, Neumann, or flux boundary conditions are specified at the inflow or outflow parts of the boundary.

2.1. Partition and Characteristic Tracking. Eulerian-Lagrangian localized adjoint methods (ELLAM) have previously been developed using triangular and quadrilateral discretizations of the domain [15, 28]. However, in this section we consider a hexagonal discretization, which for simplicity of presentation, we take to be a regular grid. The method uses a time-stepping algorithm, and so, we use the temporal partition

$$(2) \qquad\qquad t^n = n\,\Delta t, \quad n = 0,\ ...,\ N \quad \text{with } \Delta t = T/N$$

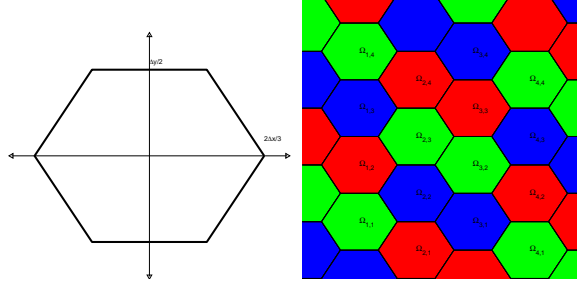for positive integer N and only focus on the current time interval $(t^n, t^{n+1}]$.

FIGURE 1. The spatial partition: the reference hexagon (left) and
a representative regular hexagonal partition of the domain (right)

The regular hexagonal grid considered, based on translations of a reference regular hexagon, is one of three possible regular tessellations of the plane, the other two being based on square and triangular tiling. It is obtained by considering a standard hexagon Ω_o centered on the origin and given by the points

$$(x_k, y_k) = \left(2\Delta x \cos\left(2\pi k/6\right)/3, \Delta y \sin(2\pi k/6)/\sqrt{3} \right), \ k = 0,..,5$$

where Δx and Δy are the discretization sizes in the x and y directions, respectively. The different elements Ω_{ij} of the spatial partition of the domain are simply given as translations of Ω_o to new centers given by

$$(x_i^c, y_j^c) = (a + i\Delta x, c + j\Delta y - \mathrm{rem}(i+1,2)\Delta y/2)$$

where $i = 0,..,n_x$, $j = 0,..,n_y$ for positive integers n_x and n_y and $\mathrm{rem}(i,2)$ is the remainder when i is divided by 2. An illustration of the partition and of the reference hexagon is given in Figure (1).

By multiplying equation (1) by a piecewise smooth test function w that vanishes outside $\Omega \times (t^n, t^{n+1}]$ we obtain a weak form of equation (1)

$$
\begin{aligned}
(3) \quad & \int_\Omega (\phi\, u)(\mathbf{x}, t^{n+1})\, w(\mathbf{x}, t^{n+1})\, d\mathbf{x} + \int_{t^n}^{t^{n+1}} \int_\Omega (\mathbf{D}\nabla u) \cdot \nabla w\, d\mathbf{x}\, dt \\
& - \int_{t^n}^{t^{n+1}} \int_\Omega u(\phi\, w_t + \mathbf{v} \cdot \nabla w)\, d\mathbf{x}\, dt + \int_{t^n}^{t^{n+1}} \int_{\partial\Omega} (\mathbf{v}\, u - \mathbf{D}\nabla u)\, w \cdot \mathbf{n}\, dS \\
& = \int_\Omega (\phi\, u)(\mathbf{x}, t^n)\, w(\mathbf{x}, t^n{}_+)\, d\mathbf{x} + \int_{t^n}^{t^{n+1}} \int_\Omega f\, w\, d\mathbf{x}\, dt
\end{aligned}
$$

where $w(\mathbf{x}, t^n{}_+) = \lim_{t \to t^n} w(\mathbf{x}, t)$ which takes into account the fact that w is discontinuous in time at time t^n.

The selection of the test function w plays an important role in the development of the methods. Using the ELLAM framework [6], we select the test functions $w(\mathbf{x}, t)$ in equation (3) to satisfy, within the tolerance of the accuracy desired, the homogeneous equation of hyperbolic part of the adjoint equation of (1)

$$(4) \qquad\qquad\qquad \phi\, w_t + \mathbf{v} \cdot \nabla w = 0$$

to reflect the Lagrangian nature of equation (1); in other words, the test functions should be chosen to be constant along the characteristics curves. These characteristic curves of equation (1) are defined as solutions to initial value problems for the ordinary differential equation

$$(5) \qquad\qquad\qquad \frac{d\mathbf{x}}{dt} = \mathbf{v}_\phi(\mathbf{x}, t) := \left(\frac{\mathbf{v}(\mathbf{x}, t)}{\phi(\mathbf{x}, t)} \right)$$

However, solving this equation for a generic velocity field is not possible, in general. Thus, we need to use some numerical means to track the characteristics approximately. A variety of algorithms may be used for that purpose, including the Euler and Runge-Kutta methods. In our formulations we use a second order Runge-Kutta method and define the approximate characteristic curve $X(\theta; \bar{\mathbf{x}}, \bar{t})$ emanating from a point $(\bar{\mathbf{x}}, \bar{t})$ by

$$(6) \qquad X(\theta; \bar{\mathbf{x}}, \bar{t}) = \bar{\mathbf{x}} + \frac{\theta - \bar{t}}{2} \left(\mathbf{v}_\phi(\bar{\mathbf{x}}, \bar{t}) + \mathbf{v}_\phi(\bar{\mathbf{x}} - (\theta - t)\mathbf{v}_\phi(\bar{\mathbf{x}}, \bar{t}), \bar{t}) \right)$$

Here θ is the time position along that characteristic. Moreover, to further improve the accuracy of tracking, we divide the global step Δt into a number of micro time steps, and the tracking described by Eq. (6) can be carried out across these micro steps.

2.2. The Reference Equation. The ELLAM method can be formulated by evaluating the space-time integrals in Eq. (3) along the approximate characteristics. Special attention needs to be given to the two triple integrals in this weak form: the second (source and sink) term on the right-hand side of the equation and the second (diffusion) term on the left-hand side. These integrals, in a similar way to all other terms, are changed to the characteristic variables, and then a backward Euler quadrature along the characteristics is applied. This results in the following formulation for the ELLAM scheme,

$$
\begin{aligned}
(7) \quad & \int_\Omega \phi(\mathbf{x}, t^{n+1}) \, u(\mathbf{x}, t^{n+1}) \, w(\mathbf{x}, t^{n+1}) \, d\mathbf{x} \\
& \quad + \int_\Omega \Delta t^{(I)}(\mathbf{x})(\mathbf{D}\nabla u)(\mathbf{x}, t^{n+1}) \cdot \nabla w(\mathbf{x}, t^{n+1}) \, d\mathbf{x} \\
& \quad + \int_{t^n}^{t^{n+1}} \int_{\partial\Omega^{(O,n)}} \Delta t^{(O)}(\mathbf{x}, t)(\mathbf{D}\nabla u) \cdot \nabla w \, (\mathbf{v} \cdot \mathbf{n}) \, dS \\
& \quad - \int_{t^n}^{t^{n+1}} \int_\Omega u \, (\phi \, w_t + \mathbf{v} \cdot \nabla w) \, d\mathbf{x} \, dt + \int_{t^n}^{t^{n+1}} \int_{\partial\Omega} (\mathbf{v}u - \mathbf{D}\nabla u) \cdot \mathbf{n} \, w \, dS \\
& = \int_\Omega \phi(\mathbf{x}, t^n) \, (\mathbf{x}, t^n) \, w(\mathbf{x}, t^n_+) \, d\mathbf{x} + \int_\Omega \Delta t^{(I)} f(\mathbf{x}, t^{n+1}) \, w(\mathbf{x}, t^{n+1}) \, d\mathbf{x} \\
& \quad + \int_{t^n}^{t^{n+1}} \int_{\partial\Omega^{(O,n)}} \Delta t^{(O)}(\mathbf{x}, t) f \, w \, (\mathbf{v} \cdot \mathbf{n}) \, dS + E(u, w)
\end{aligned}
$$

where $\partial\Omega^{(O,n)}$ is the outflow part of the boundary, $E(u, w)$ is the truncation error due to the use of Euler Quadrature, $\Delta t^{(I)}\mathbf{x} = t^{n+1} - t^*(\mathbf{x})$ where $t^*(\mathbf{x})$ is the time instance when the characteristic emanating from $(\mathbf{x}, t^{n+1})$ intersects the boundary $\partial\Omega \times [t^n, t^{n+1}]$, and similarly $\Delta t^{(O)}(\mathbf{x}, t) = t - t^*(\mathbf{x}, t)$, where $t^*(\mathbf{x}, t)$ is the time instance when the characteristic emanating from $(\mathbf{x}, t)$ intersects the boundary; both time steps extend to Δt when the corresponding characteristics do not intersect the boundary.

3. Numerical Approximation

The numerical schemes can use arbitrarily high-order trial and test functions. Here we present the scheme which uses Wachspress-type rational functions over the regular hexagonal grid presented earlier. Wachspress has pioneered the use of rational interpolation functions as basis for the test and trial spaces in finite element formulations over general convex n-gons [7, 18]. We use his formulation in our algorithm and define each global test function $w = w^{(m)}$, with m ranging over the nodes, as a piecewise rational function which has the value 1 at node m and is
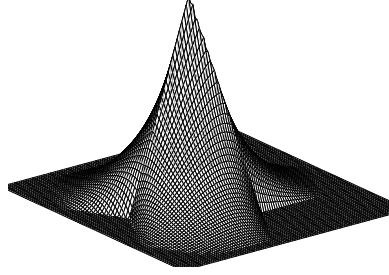
FIGURE 2. A representative global basis functions at time t^{n+1}

zero on other nodes of the partition. In particular, the local element test functions w_k are rational functions that can be written as

$$w_k(x, y, t^{n+1}) = \frac{P_k(x, y)}{Q(x, y)}$$

where the numerator is a full quartic polynomial and the denominator is a full cubic polynomial over the element. We describe below how these polynomials are obtained over the reference hexagon Ω_o. We start by labeling the sides of the reference hexagon Ω_o as $S_k, k = 1, .., 6$ where S_k connects node (x_{k-1}, y_{k-1}) to (x_k, y_k) using the convention that (x_0, y_0) is the same point as (x_6, y_6). We then define

$$a_k = \frac{y_k - y_{k-1}}{x_{k-1} y_k - x_k y_{k-1}} \text{ and } b_k = \frac{x_{k-1} - x_k}{x_{k-1} y_k - x_k y_{k-1}}$$

and define the functions

$$l_k(x, y) = 1 - a_k x - b_k y$$

each of which intercepts the xy-plane in Ω_o at the line S_k. We also define, the coefficients

$$\sigma_k = \begin{cases} 1, & k = 1 \\ \sigma_{k-1} \dfrac{a_{k+1}(x_{k-1} - x_k) + b_{k+1}(y_{k-1} - y_k)}{a_{k-1}(x_k - x_{k-1}) + b_{k-1}(y_k - y_{k-1})}, & k = 2, .., 6. \end{cases}$$

The numerator polynomials on element Ω_o are defined as

$$P_k(x, y) = \sigma_k \prod_{j=1, j \neq k, j \neq k+1}^{6} l_i(x, y)$$

while the denominator polynomial is

$$Q(x, y) = \sum_{k=1}^{6} P_k(x, y).$$

By substituting the coordinate values of the six edges of the reference hexagon Ω_o we obtain an explicit representation of the local test functions. For example,

$$w_1(x, y) = \frac{1}{6} \frac{(2\Delta x \Delta y + 3x\Delta y - 2y\Delta x)(2\Delta x \Delta y + 3x\Delta y + 2y\Delta x)(\Delta y^2 - 4y^2)}{(\Delta y^2 (4\Delta x^2 \Delta y^2 - 4y^2 \Delta x^2 - 3x^2 \Delta y^2))}$$

and the other functions are similar. Figure (2) contains a representative global basis function at time t^{n+1} which is non-zero over three adjacent elements. The method uses similar discretization and similar basis functions at the outflow boundary of

the space-time domain. Here we recall that in the interior of the space-time domain, these test functions extend to be constant along the approximate characteristics.

The numerical scheme is based on approximating the exact solution u of equation (1) (or equivalently the reference equation (7)) by a piecewise rational trial function U from the same space as the test functions. Incorporating the trial and test functions above into the reference equation (7) and dropping the truncation error term $E(u, w)$ and the adjoint term, the fourth term on the left side of the equation, gives the corresponding ELLAM schemes

$$
\begin{aligned}
(8) \quad & \int_\Omega \phi(\mathbf{x}, t^{n+1})\, U(\mathbf{x}, t^{n+1})\, w(\mathbf{x}, t^{n+1})\, d\mathbf{x} \\
& \quad + \int_\Omega \Delta t^{(I)}(\mathbf{x})(\mathbf{D}\nabla U)(\mathbf{x}, t^{n+1}) \cdot \nabla w(\mathbf{x}, t^{n+1})\, d\mathbf{x} \\
& \quad + \int_{t^n}^{t^{n+1}} \int_{\partial\Omega^{(O,n)}} \Delta t^{(O)}(\mathbf{x}, t)(\mathbf{D}\nabla U) \cdot \nabla w\, (\mathbf{v} \cdot \mathbf{n})\, dS \\
& \quad + \int_{t^n}^{t^{n+1}} \int_{\partial\Omega} (\mathbf{v}U - \mathbf{D}\nabla U) \cdot \mathbf{n}\, w\, dS \\
& = \int_\Omega \phi(\mathbf{x}, t^n)\, (\mathbf{x}, t^n)\, w(\mathbf{x}, t^n_+)\, d\mathbf{x} + \int_\Omega \Delta t^{(I)} f(\mathbf{x}, t^{n+1})\, w(\mathbf{x}, t^{n+1})\, d\mathbf{x} \\
& \quad + \int_{t^n}^{t^{n+1}} \int_{\partial\Omega^{(O,n)}} \Delta t^{(O)}(\mathbf{x}, t) f\, w\, (\mathbf{v} \cdot \mathbf{n})\, dS.
\end{aligned}
$$

With the known solution $U(\mathbf{x}, t^n)$ from the computations at the previous time step t^n (or the initial condition) and the prescribed boundary conditions, the method solves for $U(\mathbf{x}, t^{n+1})$ with $\mathbf{x}$ in Ω and also for $(\mathbf{x}, t)$ for points in $\Omega^{(O,n)}$. The scheme symmetrize the governing equation (1), generates accurate numerical solutions even if large time steps are used, and conserves mass [6].

4. Numerical Experiments

We have performed numerical experiments with the Eulerian-Lagrangian localized adjoint method developed and a report of these is presented in this section. Our aim is to observe the performance of the method in solving the model equation using classical advection dominated test problems, with known analytical solution, which are known to present numerical challenges to the simulators. We also examine the convergence of the solutions of the ELLAM method.

4.1. Convergence Rates. In this first example, we investigate the convergence rates of the ELLAM method in space and in time. As a model problem, we consider the transport of a rotating Gaussian pulse with an initial configuration given by

$$
(9) \qquad u_0(x, y) = \exp\left(-\frac{(x - x_c)^2 + (y - y_c)^2}{2\sigma^2}\right)
$$

where the center and the standard deviation are $(x_c, y_c) = (0, -0.125)$ and $\sigma = 0.015$. Equation (1) is solved with this initial condition over a domain of $\Omega = [-0.25, 0.25] \times [-0.25, 0.25]$ for a time period of $T = \pi/2$. The rotating velocity field is $\mathbf{v}(x, y, t) = \langle -4y, 4x \rangle$ which has the effect of rotating the initial configuration counter-clockwise about the origin one complete rotation during the period of the simulation. To complete the model, we select $\phi = 1$, the diffusion tensor $\mathbf{D} = 0.00005\mathbf{I}_2$ (where $\mathbf{I}_2$ is the 2×2 identity matrix), and consider a zero source/sink term. The exact solution to this problem is given by

$$
(10) \qquad u(x, y, t) = \frac{2\sigma^2}{2\sigma^2 + 4(0.00005)t} \exp\left(-\frac{(\bar{x} - x_c)^2 + (\bar{y} - y_c)^2}{2\sigma^2 + 4(0.00005)t}\right).
$$

Δh	Δt	$\mathcal{L}_2$ Error	$\mathcal{L}_1$ Error
1/30	$\pi/400$	1.0551×10^{-2}	1.2733×10^{-3}
1/36	$\pi/400$	8.7531×10^{-3}	9.4515×10^{-4}
1/42	$\pi/400$	7.1074×10^{-3}	7.1311×10^{-4}
1/48	$\pi/400$	5.5788×10^{-3}	5.2520×10^{-4}
1/54	$\pi/400$	4.0618×10^{-3}	3.7413×10^{-4}
1/60	$\pi/400$	2.7999×10^{-3}	2.5284×10^{-4}
1/66	$\pi/400$	2.1010×10^{-3}	1.8050×10^{-4}
Order of convergence α		2.06	2.47
Constant C_α		13.657	6.447

TABLE 1. Order of convergence in space achieved for the transport of the Gaussian pulse problem

Δh	Δt	$\mathcal{L}_2$ Error	$\mathcal{L}_1$ Error
1/150	$\pi/10$	2.6899×10^{-4}	1.6964×10^{-5}
1/150	$\pi/12$	2.1451×10^{-4}	1.3466×10^{-5}
1/150	$\pi/14$	1.7427×10^{-4}	1.0811×10^{-5}
1/150	$\pi/16$	1.4903×10^{-4}	8.9345×10^{-6}
1/150	$\pi/18$	1.3907×10^{-4}	8.1372×10^{-6}
1/150	$\pi/20$	1.1767×10^{-4}	6.7106×10^{-6}
1/150	$\pi/22$	1.0710×10^{-4}	6.1496×10^{-6}
Order of convergence β		1.16	1.30
Constant C_β		0.001008	0.000076

TABLE 2. Order of convergence in time achieved for the transport of the Gaussian pulse problem

where $(\bar{x}, \bar{y}) = (x \cos 4t + y \sin 4t, -x \sin 4t + y \cos 4t)$.

The truncation error of the ELLAM schemes can be estimated as follows

$$(11) \qquad \max_{n=0,..,N} \|u(\mathbf{x}, t^n) - U(\mathbf{x}, t^n)\|_{\mathcal{L}_P} \leq C_\alpha (\Delta h)^\alpha + C_\beta (\Delta t)^\beta$$

in the $\mathcal{L}_2$ and the $\mathcal{L}_1$ norms where $\Delta x = \Delta y =: \Delta h$; here α and β are the orders of convergence in space and time, respectively [19]. We carry different runs to numerically investigate the rates α and β that we obtain for the rational ELLAM method. We first vary the spatial grid size Δh systematically with the temporal step being sufficiently refined so that the temporal errors are negligible. We then use a linear regression to fit the spatial convergence rates. Table (1) contains the $\mathcal{L}_2$ and the $\mathcal{L}_1$ norms of the errors generated by the ELLAM scheme for this test problem. Similarly we simulate the problem using a fixed spatial grid with a relatively fine
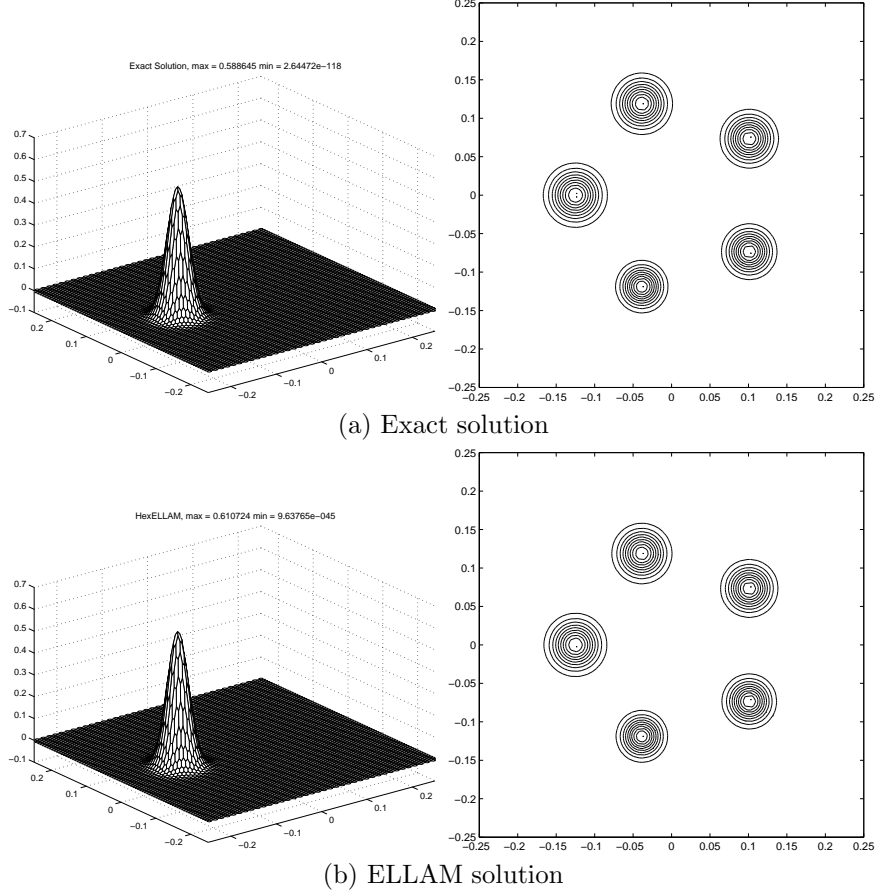
Exact Solution, max = 0.588645 min = 2.64472e−118

(a) Exact solution

HexELLAM, max = 0.610724 min = 9.63765e−045

(b) ELLAM solution

FIGURE 3. Plots at $t = \pi/2$ and contours at $t = \pi/10$, $\pi/5$, $3\pi/10$, $2\pi/5$, $\pi/2$ of the exact solution and the ELLAM solution with $\Delta x = \Delta y = 1/150$ and $\Delta t = \pi/10$ for the transport of a Gaussian pulse problem

size and use temporal grids of various sizes to investigate the convergence in time. The results of these runs are given in Table (2). The results obtained collectively suggest optimal-order convergence rates in space and time for the ELLAM solutions in the two norms, which are yet to be proved theoretically. Here we also remark that the constant C_β is much smaller than C_α, which is mainly due to the fact that the temporal truncation errors are significantly reduced when Lagrangian tracking is employed in the simulation, an advantage of characteristic methods, in general.

The choice of the relatively small time steps Δt in Table (1) was to establish the order of convergence. However, one main advantage of ELLAM and characteristic methods in general is that they allow large time steps to be used in the simulations as it is evident in the results presented in Table (2). Therefore, in Figure (3), we present the solution generated by the ELLAM method for this model problem using a grid of size $\Delta h = 1/150$ and the relatively larger $\Delta t = \pi/10$. The ELLAM method performs very well, comparably to existing polynomial interpolation based ELLAM methods, and presents a solution with relatively small absolute errors of magnitude 2.6899×10^{-4} and 1.6964×10^{-5} in the $\mathcal{L}_2$ and $\mathcal{L}_1$norms, respectively.

4.2. Transport of a Diffused Box Function. In order to test the ELLAM method developed for problems with discontinuous initial data, we consider in this example the transport of a diffused rectangular box function with initial configuration given by

$$u_0(x,y) = \begin{cases} 1, & (x,y) \in [x_l, x_r] \times [y_l, y_r] \\ 0, & \text{otherwise} \end{cases} \tag{12}$$

subject to equation (1), where $x_l = -0.08005$, $x_r = -0.4495$, $yl = -0.01755$ and $y_r = 0.01755$. In this problem we consider a spatial domain of $[-0.125, 0.125] \times [-0.125, 0.125]$ and simulate for a time period of $T = \pi/2$. The other parameters used in this experiment are the same as those used in the previous test problem with the exception that we use an even smaller diffusion tensor of $\mathbf{D} = 0.00002 \times \mathbf{I}_2$. The exact solution of this model problem is given by

$$u(x,y,t) = \frac{1}{4}\left[\operatorname{erf}\left(\frac{\bar{x}-x_l}{\sqrt{0.00008t}}\right) - \operatorname{erf}\left(\frac{\bar{x}-x_r}{\sqrt{0.00008t}}\right)\right] \times \tag{13}$$
$$\left[\operatorname{erf}\left(\frac{\bar{y}-y_l}{\sqrt{0.00008t}}\right) - \operatorname{erf}\left(\frac{\bar{y}-y_r}{\sqrt{0.00008t}}\right)\right]$$

where $\operatorname{erf}(x) = 2/\sqrt{\pi}\int_0^x e^{-s^2}ds$ is the standard error function, and $(\bar{x},\bar{y}) = (x\cos 4t + y\sin 4t, -x\sin 4t + y\cos 4t)$ as defined earlier.

Δh	Δt	$\mathcal{L}_2$ Error	$\mathcal{L}_1$ Error
1/320	$\pi/10$	4.4506×10^{-4}	2.3366×10^{-5}
1/320	$\pi/20$	1.9744×10^{-4}	1.0249×10^{-5}

TABLE 3. Representative results for the transport of a diffused box function test problem

In Table (3) we present the numerical results of some representative example runs, while in Figure (4), we present plots of the ELLAM solution using a grid of sizes $\Delta x = 1/320$ and $\Delta t = \pi/10$ as well as the exact solution. These results show that the ELLAM scheme very accurately captures the details and the steep fronts of the exact solution, in a comparable manner to that experienced with polynomial based characteristic methods. These results justify the appropriateness of these rational basis and the high-order elements within the set-up of ELLAM methods.

4.3. Diffusion in a plane shear flow. The third set of experiments we carry involves the transport under the influence of a shear flow and was presented by Carter *et al* [5]. The model equation (1) is solved using a velocity field of $\mathbf{v}(x,y,t) = \langle 1 + 2y, 0 \rangle$ and a diffusion of $\mathbf{D} = 0.0001\mathbf{I}_2$ over a spatial domain of $[0, 1.3] \times [-0.2, 0.2]$. The analytic solution subject to an initial condition of $M\delta(x_0, 0)$ (where δ represents the dirac delta function) is given by

$$u(x,y,t) = \frac{M}{0.0004\pi t\sqrt{1+\frac{4t^2}{12}}} \exp\left(-\frac{(x-x_0-t-yt)^2}{0.0004t(1+\frac{4t^2}{12})} - \frac{y^2}{0.0004t}\right)$$

where we have used the value $M = 0.002$ and $x_0 = 0$.

In the model problem we work with a finite initial condition at $t = 0.2$ and simulate over the time interval $[0.2, 1.2]$. As a representative model run, we simulate the problem with a discretization of $\Delta x = \Delta y = 1/100$ and $\Delta t = 1/10$ and present
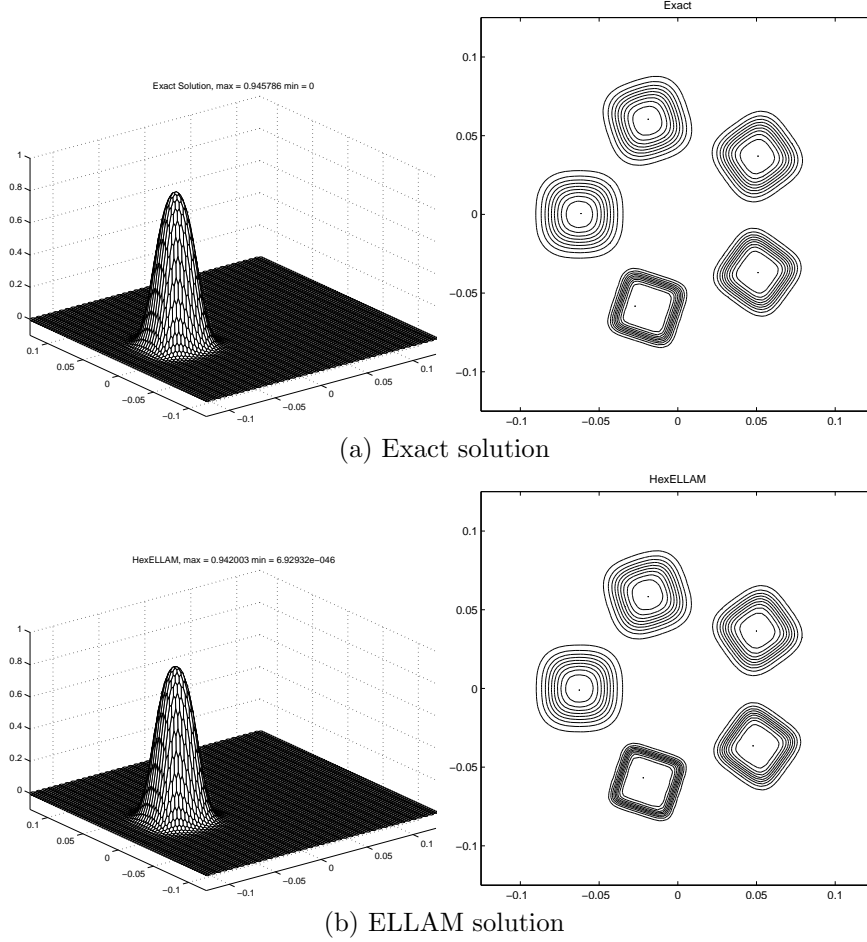
(a) Exact solution

(b) ELLAM solution

FIGURE 4. Plots at $t = \pi/2$ and contours at $t = \pi/10$, $\pi/5$, $3\pi/10$, $2\pi/5$, $\pi/2$ of the exact solution and the ELLAM solution with $\Delta x = \Delta y = 1/320$ and $\Delta t = \pi/10$ for the transport of a box function problem

Δh	Δt	$\mathcal{L}_2$ Error	$\mathcal{L}_1$ Error
1/100	1/5	1.0578×10^{-3}	7.4238×10^{-5}
1/100	1/10	6.0565×10^{-4}	4.1167×10^{-5}
1/100	1/15	5.3671×10^{-4}	3.6175×10^{-5}

TABLE 4. Representative results for the diffusion in a plane shear flow test problem

the ELLAM solution along with the analytic solution in Figure (5). The norms of the errors of the solutions generated by the ELLAM scheme are an $\mathcal{L}_2$ norm of 6.0565×10^{-4} and an $\mathcal{L}_1$ norm of 4.1167×10^{-5} (see Table (4)).
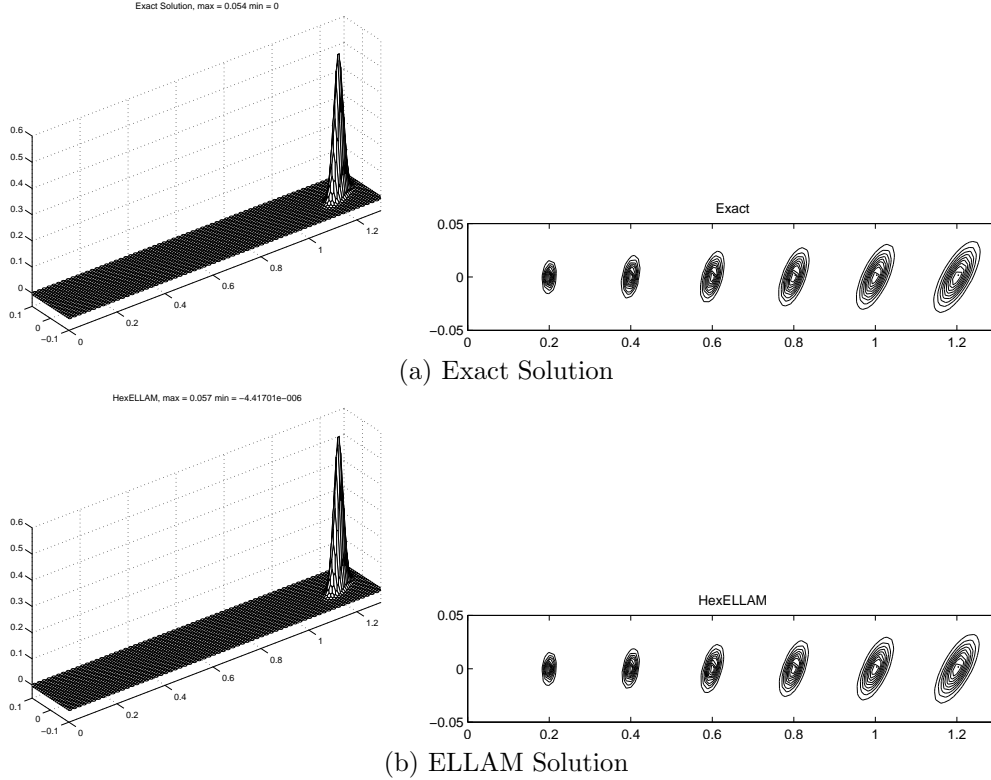
(a) Exact Solution

(b) ELLAM Solution

FIGURE 5. Plots of the initial condition and the solution at $t = 1.2$ and contours at $t = 0.2, 0.4, 0.6, 0.8, 1.0\ 1.2$ of the exact solution and the ELLAM solution with $\Delta h = 1/100$ and $\Delta t = 1/10$

5. Discussion

In this article we develop a characteristic method which uses piecewise Wachspress type rational test and trial functions over regular hexagonal grid within the framework of the Eulerian-Lagrangian localized adjoint methods. The derived scheme performs well and generates accurate numerical solutions even when large time steps are used in the simulation. Numerical experiments illustrate the strong potential of the derived scheme and clearly justify the appropriateness of the hexagonal grids and the piecewise rational basis functions within the framework of the ELLAM method. Moreover, they show a strong potential for practical use and a wide industrial applicability. When compared to the polynomial-based ELLAM methods, the derived scheme performs comparably well. However, no comparison is presented in this article mainly because polynomial interpolations may not be very suitable over such hexagonal grids. This comparison in other more appropriate settings for both types of interpolations will be a topic for future investigation.

The extension of the rational ELLAM method to three dimensional problems is theoretically possible, especially since generalization of the Wachspress construction to three space dimensions have been considered [38]. This extension will also be a topic for future investigation.

References

[1] M. Al-Lawatia, R.C. Sharpley, and H. Wang, Second-order characteristics methods for advection-diffusion equations and comparison to other schemes, *Advances in Water Resources*, **22** (1999) 741-768.

[2] M. Al-Lawatia, H. Wang, A family of higher-order ELLAM method for advection-diffusion equations,*AMS Contemporary Mathematics*, 295:25-35, 2002

[3] P.J. Binning, and M.A. Celia, A Forward Particle Tracking Eulerian Lagrangian Localized Adjoint Method for Solution of the Contaminant Transport Equation in Three Dimensions, *Advances in Water Resources*, 25:147-157, 2002.

[4] E.T. Bouloutas and M.A. Celia, An improved cubic Petrov-Galerkin method for simulation of transient advection-diffusion processes in rectangularly decomposable domains,*Comp. Meth. Appl. Mech. Engrg.* 91:289-308, 1991.

[5] H. Carter and A. Okubo, A study of the physical processes of movement and dispersion in the Cape Kennedy area, Chesapeake Bay Inst. Ref 65-2, Johns Hopkins Univ., Baltimore, MD, 1965.

[6] M.A. Celia, T.F. Russell, I. Herrera, and R.E. Ewing, An Eulerian-Lagrangian localized adjoint method for the advection-diffusion equation, *Advances in Water Resources* 13:187–206, 1990.

[7] G. Dasgupta, Interpolants within Convex Polygons: Wachspress Shape Functions, *Journal of Aerospace Engineering* 16(1):1-8, 2003.

[8] C.N. Dawson, Godunov-mixed methods for advective flow problems in one space dimension, *SIAM J. Numer. Anal.* 28:1282–1309, 1991.

[9] J. Douglas, Jr. and T.F. Russell, Numerical methods for convection-dominated diffusion problems based on combining the method of characteristics with finite element or finite difference procedures, *SIAM J. Numer. Anal.* 19:871-885, 1982.

[10] C. I. Heberton, T.F. Russell, L.F. Konikow, and G.Z. Hornberger, A three-dimensional finite-volume Eulerian-Lagrangian localized adjoint method (ELLAM) for solute-transport modeling, USGS water-resources invstigation report 00-4087, Reston, Virginia, 2000

[11] T.J.R. Hughes and M. Mallet, A new finite element formulation for computational fluid dynamics III, The general Streamline operator for multidimensional advective-diffusive systems, *Comp. Meth. Appl. Mech. Engrg.* 58:305–328, 1986.

[12] C. Johnson, Numerical solution of partial differential equations by the finite element method, Cambridge University Press, Cambridge, 1987.

[13] O. Pironneau, On the transport-diffusion algorithm and its application to the Navier-Stokes equations, *Numer. Math.* 38:309-33, 1982.

[14] T.F. Russell and R.V. Trujillo, Eulerian-Lagrangian localized adjoint methods with variable coefficients in multiple dimensions, in: Gambolati, et al (eds.), Computational Methods in Surface Hydrology 357–363, Springer-Verlag, Berlin, 1990.

[15] J. Liu, H. Chen, R. Ewing and G. Qin, An efficient algorithm for characteristic tracking on two-dimensional triangular meshes, *Computing* 80, 121136 (2007).

[16] X.-D. Liu, S. Osher, and T. Chan, Weighted essentially nonoscillatory schemes, *J. Comput. Phys.* 115:200–212, 1994.

[17] B. van Leer, On the relation between the upwind-differencing schemes of Godunov, Engquist-Osher and Roe, *SIAM J. Sci. Statist. Comput.* 5:1–20, 1984.

[18] E.L. Wachspress, A rational finite element basis, Academic, New York, 1975.

[19] H. Wang, A family of ELLAM schemes for advection-diffusion-reaction equations and their convergence analyses, *Numerical Methods for PDEs* 14:739–780, 1998.

[20] H. Wang, An optimal-order error estimate for an ELLAM scheme for two-dimensional linear advection-diffusion equations, *SIAM J. Numer. Anal.* 37, 1338–1368, 2000.

[21] H. Wang, An optimal-order error estimate for MMOC and MMOCAA schemes for multidimensional advection-reaction equations, *Numerical Methods for PDEs*, 18(2002), 69–84.

[22] H. Wang, An optimal-order error estimate for a family of ELLAM-MFEM approximations to porous medium flow,*SIAM J. Numer. Anal.* 46: 2133–2152, 2008

[23] H. Wang, R.E. Ewing, and T.F. Russell, Eulerian-Lagrangian localized methods for convection-diffusion equations and their convergence analysis, *IMA J. Numer. Anal.*, 15: 405–459, 1995.

[24] H. Wang, X. Shi and R.E. Ewing, An ELLAM scheme for multidimensional advection-reaction equations and its optimal-order error estimate,*SIAM. J. Numer. Anal.*, 38: 1846–1885, 2001.

[25] H. Wang and K. Wang, Uniform estimates for Eulerian-Lagrangian methods for singularly perturbed time-dependent problems, *SIAM J. Numer. Anal.*, 45: 1305–1329, 2007.

[26] H. Wang, M. Al-Lawatia, and A.S. Telyakovskiy, A Runge-Kutta characteristic method for first-order linear hyperbolic equations, *Numerical Methods for PDEs*, 13:617-661, 1997

[27] H. Wang and M. Al-Lawatia, A locally conservative Eulerian-Lagrangian control-volume method for transient advection-diffusion equations, *Numerical Methods for PDEs* 22:2005.

[28] H. Wang, R.E. Ewing, G. Qin, S.L. Lyons, M. Al-Lawatia, S. Man, A family of Eulerian-Lagrangian localized adjoint methods for multi-dimensional advection-reaction equations. *J. Comput. Phys.*, **152** (1999) 120–163

[29] H. Wang, H., H.K. Dahle, R.E. Ewing, M.S. Espedal, R.C. Sharpley, and S. Man, An ELLAM scheme for advection-diffusion equations in two dimensions, *SIAM J. Sci. Comput.* 20: 2160-2194, 1999.

[30] K. Wang, A uniformly optimal-order error estimate of an ELLAM scheme for unstady-state advection-diffusion equations, *International journal of numerical analysis and modeling* 5: 286–302, 2008.

[31] K. Wang and H. Wang, A Uniform Estimate for the ELLAM Scheme for Transport Equations, *Numerical Methods for PDEs* 24: 535–554, 2008.

[32] K. Wang and H. Wang, An optimal-order error estimate to the modified method of characteristics for a degenerate convection-diffusion equation, *International Journal of Numerical Analysis and Modeling* 6: 217–231, 2009.

[33] K. Wang and H. Wang, A uniform estimate for the MMOC for two-dimensional advection-diffusion equations, *Numerical Methods for PDEs* Published Online: May 27, 2009.

[34] K. Wang, A uniform optimal-order estimate for an Eulerian-Lagrangian discontinuous Galerkin method for transient advection-diffusion equations,*Numerical Methods for PDEs* 25: 1283-1302, 2009.

[35] K. Wang, H. Wang, and M. Al-Lawatia, An Eulerian-Lagrangian discontinuous Galerkin method for transient advection-diffusion equations, *Numer. Methods for Partial Differential Equations* 23: 1343–1367, 2007.

[36] K. Wang, H. Wang, and M. Al-Lawatia, A CFL-free explicit characteristic interior penalty scheme for linear advection-reaction equations, *Numer. Methods for PDEs*, Published Online: Mar 19, 2009, DOI: 10.1002/num.20447.

[37] K. Wang, H. Wang, M. Al-Lawatia, and H. Rui, A family of characteristic discontinuous Galerkin methods for transient advection-diffusion equations and their optimal-order L^2 error estimates,*Communications in Computational Physics* 6 (2009), 203–230.

[38] J. Warren, S. Schaffer, A. Hirani, and M. Desbrun, Barycentric Coordinates for Convex Sets, Tech. rep., Rice University, 2004.

[39] L. Wu and H. Wang, An Eulerian-Lagrangian single-node collocation method for transient advection-diffusion equations in multiple space dimensions, *Numerical Methods for Partial Differential Equations* 20: 284–301, 2004.

[40] L. Wu, H. Wang, and G.F. Pinder, A nonconventional Eulerian-Lagrangian single-node collocation method with Hermite polynomials for unsteady-state advection-diffusion equations, *Numerical Methods for PDEs* 19: 271–283, 2003.

[41] L. Wu and K. Wang, A single-node characteristic collocation method for unsteady-state convection-diffusion equations in three-dimensional spaces, *Numerical Methods for PDEs*, Pulished online,DOI: 10.1002/num.20552.

Department of Mathematics and Statistics, Sultan Qaboos University, P.O. Box 36, Al-Khod 123, Sultanate of Oman

E-mail: `allawati@squ.edu.om`

URL: `http://www.squ.edu.om/Portals/87/StaffHome/4284/4284.html`